ACS Photonics

Article

pubs.acs.org/journal/apchd5

Efficient Platform for Flexible Engineering of Superradiant, Fano-Type, and Subradiant Resonances

Bo-Wen Liu,[†,‡] Xu Yao,[†] Liang Zhang,[∥] Hai-Xin Lin,[†] Shu Chen,[⊥] Jin-Hui Zhong,[†,§] Shou Liu,[†] Lei Wang,[*,∥] and Bin Ren[*,†,‡,§]

[†]State Key Laboratory of Physical Chemistry of Solid Surfaces and College of Chemistry and Chemical Engineering, [‡]The MOE Key Laboratory of Spectrochemical Analysis and Instrumentation, [§]Collaborative Innovation Center of Chemistry for Energy Materials, [∥]Department of Mechanical and Electrical Engineering, and [⊥]Department of Physics, Xiamen University, Xiamen 361005, China

Supporting Information

ABSTRACT: Delicate control of the surface plasmon resonance (SPR) line shapes is crucial for the development of nanoplasmonics with dedicated applications. In this paper, we develop a method to fabricate large-scale periodic structures with significantly different plasmonic properties by the holographic lithography method. We show that SPR line shapes can be controllably engineered from a broad superradiant line shape to an asymmetrical Fano-type resonance, as well as an ultranarrow subradiant mode, which are clearly correlated with the structural parameter (morphology) of the fabricated structures. The wavelength of the SPR band can be tuned from the visible to near-infrared region by changing the incident angle. The nanostructures fabricated by the present method show a clear correlation between the morphology of plasmonic structures and SPR line shapes, which can serve as an efficient platform for engineering SPR line shapes for specific applications. Most importantly, the capability to produce structures of large area further supports the unprecedented opportunity to push these plasmonic structures fabricated by holographic lithography toward real applications.

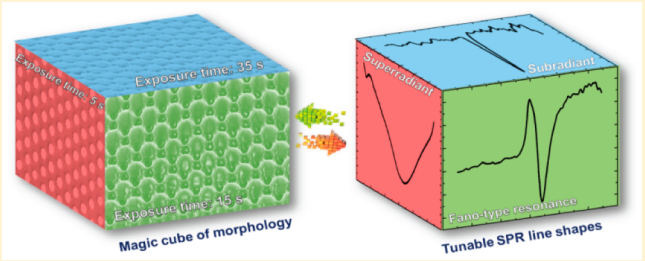

KEYWORDS: *SPR line shape, plasmon hybridization, plasmonic structure, holographic lithography*

Nanostructures with unique surface plasmon resonance (SPR) properties have attracted increasing interest, especially in the past 10 years, leading to the formation of a vibrant field of nanoplasmonics.[1−3] The properties of plasmonic materials rely significantly on their fine structures. To achieve dedicated plasmonic properties or performance, various nanostructures have been fabricated by methods ranging from bottom-up colloidal synthesis to top-down nanofabrication. It has been well documented that the material, morphology, and size of the nanostructures may affect their SPR spectral position.[4] Recently, there is an increasing interest in fabricating nanostructures with designed SPR line shapes.[5−11] The driving force is that different SPR line shapes have found different applications.[7,11−13] For instance, the narrow and sharp SPR line shape is advantageous for use as plasmonic devices, such as nanolasers,[14−16] biochemical sensors,[13,17−19] or optical switches.[2] Taking SPR sensors for example, they require an ultranarrow line shape, because the minimum detectable spectral shift is limited by the full width at half-maximum (fwhm), and a higher figure of merit (FOM) value can be obtained with a smaller fwhm.[18−20] On the other hand, for the plasmon-assisted photovoltaic devices, such as solar cells, the broad absorption spectral line shape is appreciated for a better utilization of the wide sunlight spectrum.[21−24] Furthermore, surface-enhanced spectroscopies, such as surface-enhanced Raman scattering (SERS) and surface-enhanced infrared absorption spectroscopy (SEIRAS), also require a broad SPR line shape to achieve the enhancement over a defined spectral range.[6]

An effective approach to engineer the SPR line shape is to utilize the interference (or coupling) between two or more individual SPR modes. The coupling between a broad (superradiant, continuous, or bright) mode and a narrow (subradiant, discrete, or dark) mode[25] on plasmonic structures is similar to the Fano resonance in a quantum system and is called Fano-type resonance.[2,7,9,26,27] The Fano-type resonance usually leads to the asymmetrical and narrow line shapes, which has found important applications in plasmonic sensing.[18,19,28] The SPR line shape can be further narrowed by reducing the loss of the SPR system that is caused by the intrinsic damping of metal and the radiation processes.[13,18] Other important approaches for engineering plasmon resonance include plasmon spectral decomposition[29−31] and plasmonic−photonic mode hybridization.[32] Various plasmonic structures have been fabricated and demonstrated for engineering of SPR line shapes. For instance, Fano-type resonances have been found on nonconcentric ring-disk cavities,[3] dolmen-type resonators,[12,27] finite oligomers,[9,26,33] and plasmonic metamaterials.[8,34,35] Low-loss SPR systems with ultranarrow line shapes have also been

Received: July 26, 2015
Published: November 23, 2015

DOI: 10.1021/acsphotonics.5b00650
ACS Photonics 2015, 2, 1725−1731

realized on a thin nanohole array with a reduced intrinsic damping,[18,36] as well as the double-layer nanorod structure,[8] and cavity plasmonic structures as a result of the interference between cavity mode and SPR mode,[37] while to achieve a broad SPR line shape, complex plasmonic structures with a multilayer configuration have been used.[22−24]

These theoretical and experimental results have provided important insights into the engineering of SPR line shape and have achieved the important proof-of-concept understanding. It should be pointed out that most of the current methods are either too expensive[7,8,27] or too complex[18,22] to allow a large-scale fabrication of those useful plasmonic structures. Therefore, it is desirable to develop high-throughput methods to conveniently and controllably fabricate large-area plasmonic nanostructures with tunable SPR line shapes.

Holographic lithography (HL), which is also well known as laser interference lithography,[38,39] appears to be a promising method to meet the above challenge. HL utilizes the interference of multiple coherent laser beams to produce periodic structures.[40] The interference of two coherent laser beams produces a grating structure, and interference of three beams can produces a hexagonal pattern. Therefore, HL has been widely used to fabricate two-dimensional and three-dimensional photonic crystals.[40−42] Because the structure is determined by the interference pattern of laser beams, a periodic array can be obtained over a large area with high uniformity by expanding and filtering the laser beam.[43] As a result, HL has been used to fabricate highly uniform SERS or SEIRA substrates.[44,45] More recently, HL has also been used to fabricate a nanostructured substrate with an ultranarrow SPR line shape. As a result of the narrow Fano-type resonance, the substrate showed excellent performance as a SPR sensing substrate.[18,19] However, up to now there is still no report on the attempt to tune the morphology of plasmonic structures to achieve tunable SPR line shapes by the HL method.

In this work, we utilized a home-built HL system to fabricate a series of periodic hexagonal array structures with controllable morphologies by a precise control of the exposure time during the HL process. The photoresist arrays were transformed into plasmonic structures after gold film deposition by an electron beam vacuum deposition system. We successfully obtained the SPR line shapes from the superradiant broad line shape, to the asymmetrical Fano-type line shape, and to the ultranarrow subradiant line shape on these plasmonic structures with different morphologies. In addition, the optical properties of those Au hexagonally complementary plasmonic structures are polarization and incident-angle dependent. With the ease of fabrication in a large scale and tunable SPR line shape, the fabricated plasmonic structures hold great promise for various plasmonic applications.

RESULTS AND DISCUSSION

There are two common ways in HL to achieve the interference of multiple coherent laser beams. One is to use mirrors to direct laser beams to the spatially designed position, so that the laser beams can interfere in the designed way.[40,45,46] This method requires a rigorous alignment of optical path, and therefore it is sensitive to the stability of the optical system. Alternatively, one can also use a holographic optical element (HOE) with prefabricated diffractive gratings (as shown in the left panel of Figure 1a; see also Figures S1 and S2 in the Supporting Information). When the HOE is uniformly illuminated with a single expanded laser beam, the interference

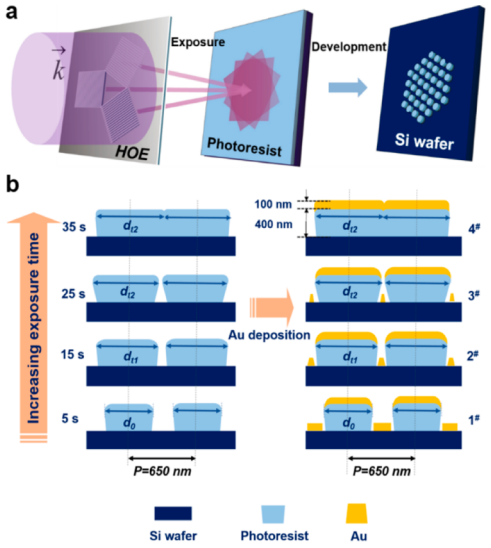

Figure 1. (a) Schematic illustration of the principle of holographic lithography. (b) Tuning the morphology of the nanostructures by controlling the exposure time: a sketch of the photoresist (left) and the gold-deposited photoresist array (right).

of the first-order laser beams of gratings will produce the designed periodic pattern. The patterned light is then applied to illuminate a substrate coated with photoresists for exposure (see middle panel of Figure 1a; see also Figure S3 in the Supporting Information). After development, the substrate will produce a periodic photoresist structure. Depending on the type of photoresists, the obtained structure may be a positive or negative copy of the pattern.

For a negative photoresist used in this work, after a single exposure, the exposed zones are left to form the final hexagonal nanopillar arrays (see right panel of Figure 1a), while the nonexposed zones are dissolved in the developing solution. Without relying on changing the optical path or further post-treatment,[44] the gap of the hexagonal nanopillar arrays can be conveniently tuned by simply controlling the dose during the exposure process (left panel of Figure 1b). In the present work, the exposure dose is tuned by changing the exposure time with a constant laser power.[41] As the exposure time can be tuned within tens of seconds, HL offers a high-throughput method in a single exposure. As illustrated in the left panel of Figure 1b, the diameter of the nanopillar will increase with the extended exposure time. Figure 2a shows a scanning electron microscopy (SEM) image of the photoresist array. It is clear that the substrate has a highly ordered structure over a large area. After the gold deposition on the photoresist template by the electron beam vacuum system, a series of plasmonic structures with varying morphologies are formed (see right panel of Figure 1b). Figure 2b displays a photo of the fabricated structure after the deposition of gold, in comparison with a coin of one Chinese yuan (ca. 2.5 cm diameter). The substrate shows a homogeneous rainbow color over a large area (ca. 1 cm diameter), indicating a high periodicity and uniformity of the structure. Therefore, the current HL method is a high-throughput approach for fabrication of uniform plasmonic structures over a large area.

In fact, both the period and morphology of the fabricated structure can be tuned by using different HOEs. The height of the photoresist pillar is determined by the thickness of the photoresist, which can be tuned by using different spin rates

DOI: 10.1021/acsphotonics.5b00650
ACS Photonics 2015, 2, 1725−1731

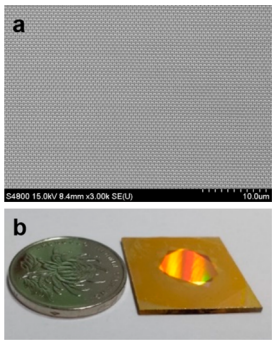

Figure 2. (a) SEM image of a typical highly uniform substrate fabricated by the HL method after the development process. (b) Photo of a typical plasmonic substrate after the deposition of 100 nm thick gold, in comparison with a coin of one Chinese yuan.

during the spin-coating process. The thickness of the gold film and type of metal can be varied during the deposition process. However, we were mainly focused on the effect of morphology on the plasmonic properties in this work. Therefore, we changed only the exposure time to achieve different morphologies and investigate the effect of morphology on the plasmonic properties. We did not make any attempt to change other parameters. Therefore, all the plasmonic structures shown in this work have a period of 650 nm, a height of the photoresist nanopillar of 400 nm, and a thickness of the gold film of 100 nm. All detailed parameters are marked in Figure 1b. Such a high flexibility in fabricating a large-area uniform substrate is one of the highlights of this work (see Figure 1b and Figure 3a–d).

The plasmonic structures obtained on a photoresist nanopillar with exposure times of 5, 15, 25, and 35 s are shown in Figure 3a–d, respectively. From the top view, the hexagonally arranged nanopillar arrays were obtained at an exposure time of 5 s (Figure 3a). With the increase of the exposure time, the diameter of the nanopillars increases and the nanopillars start to overlap with the adjacent ones to form an intermediate structure, as shown in Figure 3b and c. The touching of the neighboring nanopillars leads to the formation of nanobridges and nanoholes among the nanopillars. At the exposure time of 35 s, the adjacent nanopillars overlap with each other, and the gaps are filled, leaving only very shallow recesses (Figure 3d). Therefore, by increasing the exposure time, we can systematically increase the diameters of nanopillars so that the gaps between the adjacent pillars decrease. In fact, the differences in these plasmonic structures are more interesting from their side views. As illustrated in the right panel of Figure 1b, two gold layers are vertically separated by the photoresist nanopillar. Here, we call the top gold layer a gold cap and bottom gold layer a gold disk. With the increase of the diameter of the photoresist nanopillar, the diameter of the top gold cap increases and the bottom gold disk decreases. As will be shown later, these 3D complementary structures show interesting and significantly different optical properties.

To simplify the following discussion, we name the substrates obtained at exposure times of 5, 15, 25, and 35 s as arrays $1^{\#}$, $2^{\#}$, $3^{\#}$, and $4^{\#}$, respectively. From array $1^{\#}$ to $4^{\#}$, as shown in Figure 1b, the diameter of the photoresist pillar as well as the final gold cap increases, while the gap between the photoresist pillar and the diameter of the bottom gold disk decreases. As a result of the interaction of the SPR modes of gold caps and gold disks, different SPR line shapes were obtained on different plasmonic structures. The reflectance spectra of the plasmonic structure obtained at normal excitation (0°) and oblique excitation (30°) are shown in Figure 3e and f, respectively. Under normal excitation conditions (Figure 3e), the SPR line shapes change from broad to narrow accompanied by a blue shift of the reflectance dips from array $1^{\#}$ to $4^{\#}$. For array $4^{\#}$, the bottom gold disks vanish, leaving only the top gold cap array. On this substrate, a narrow SPR line shape was observed, which is contributed by the top gold cap array (further assignment of this mode will be discussed in the following parts). The bottom gold disks appear on array $3^{\#}$, and the size increases from array $2^{\#}$ to $4^{\#}$. Mixing of the SPR modes of the top gold cap array and the bottom gold disk array results in the broadening of the SPR line shape. The line shape becomes broader with the increasing size of the bottom gold disk array. For a p-polarized excitation at an incident angle of 30° (Figure 3g), the asymmetric excitation leads to a phase difference between the SPR modes of the top and bottom layer. As a result, a prominent change of the line shapes is observed. Similar to the normal excitation case, array $4^{\#}$ gives a narrow SPR line shape, which originates from the top gold cap array. In comparison, arrays $1^{\#}$ to $3^{\#}$ give

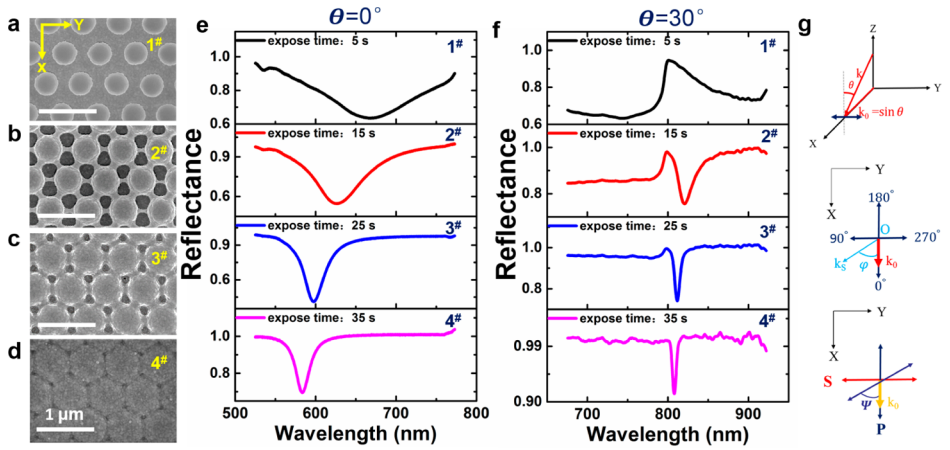

Figure 3. Fabricated plasmonic structures with engineered morphologies. The exposure time was (a) 5 s, (b) 15 s, (c) 25 s, and (d) 35 s. Experimental detected zero-order reflectance spectra of the corresponding plasmonic nanoarrays with incident angles of 0° (e) and 30° (f). (g) Schematic of excitation configuration with different incident angles θ and the definition of structural angle φ and polarization angle ψ.

DOI: 10.1021/acsphotonics.5b00650
ACS Photonics 2015, 2, 1725–1731

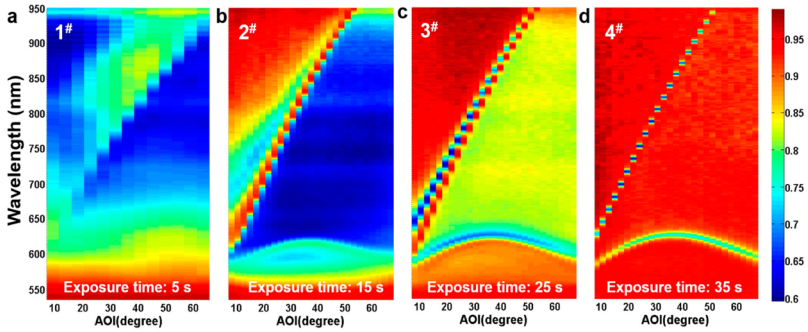

Figure 4. Incident angle-dependent reflectance spectra of the four plasmonic arrays $1^{\#}$ (a), $2^{\#}$ (b), $3^{\#}$ (c), and $4^{\#}$ (d). The excitation conditions are the same as that shown in Figure 2g.

a blue shift of spectral position and narrowing of the SPR line shape and show a line shape of a typically asymmetrical Fano-type resonance.[2] The asymmetrical line shape can be attributed to the coupling between the broad SPR mode of the bottom gold disk and the narrow SPR mode of the top layer gold cap array.[2,17,19] Therefore, by simply controlling the exposure time, we were able to obtain plasmonic nanoarrays with superradiant, subradiant, and asymmetrical Fano-type line shapes.[3,10]

Detailed analysis of the dispersive relation of these periodic plasmonic structures will be helpful to identify these SPR modes and their dependency on the corresponding plasmonic structures. For this purpose, we systematically studied the angle-dependent optical response for the four plasmonic arrays, using the same excitation condition shown in Figure 3g on our home-built angle-dependent spectroscopic system. The diameter of the collimating excitation beam was set as large as 5 mm to cover a large area of the substrate, and the angle of incidence (AOI) was measured from 7° to 70°. The results are shown in Figure 4a–d for the plasmonic nanoarrays $1^{\#}$, $2^{\#}$, $3^{\#}$, and $4^{\#}$, respectively.

As illustrated in Figure 4d, the SPR array $4^{\#}$ depends critically on the incident angle. Especially the SPR mode above 600 nm has a narrow line shape and shifts linearly from 630 nm at 7° to 950 nm at 50°. This mode can be assigned to be a surface plasmon polaritons (SPP) mode of the periodic nanocap array on the top layer, because an angle-dependent shift of the reflectance dip of this mode can be well simulated using the SPP model (see eq S1 and Figure S7 for detailed analysis). This narrow SPP mode over a large incident angle range is advantageous for the SPR sensing.[17,19,20] Arrays $2^{\#}$ and $3^{\#}$ show a Fano-type line shape (see Figure 3f and Figure 4b and c)[2,17,19] showing clear angle-dependent properties. The gold disks on the bottom layer give a broad localized surface plasmon resonance (LSPR). Such a Fano-type line shape is a result of the coupling between the narrow SPP mode of the top gold array and broad LSPR mode of the bottom gold disk. The peak position of the Fano-type resonance red shifts with the increase of the angle and matches well with the shift predicted using the SPP mode. The angle-dependent reflectance spectra on array $1^{\#}$ show a broadband line shape in the wavelength range from 650 to 950 nm. The optical property of this kind of structure is insensitive to the incidence angle. The broad line shape is retained over the whole angle range from 7° to 70°. It is worthwhile to look into the detailed structure of array $1^{\#}$, as it is much different from the other three structures. The top gold caps are separated from each other and become individual nanopoles that may act as absorptive and radiation antennas. Meanwhile, the gold disks extend to form a continuous gold nanohole film on the bottom layer, with the nanopoles sitting in the center of the nanoholes. Such a complex structure leads to a very complicated interaction among different SPR modes: the LSPR of the nanopoles, the LSPR of the nanoholes, and the SPP of the continuous gold film of the nanohole layer, which form very different reflectance spectra on array $1^{\#}$ compared with the other three structures. As the period of all the plasmonic structures is the same, the spectral position of the SPP mode will not change. With the increase of the exposure time from array $1^{\#}$ to $4^{\#}$, the size of the bottom gold disks decreases, leading to a blue shift of the LSPR position (as seen in Figure 3e).

The above results suggest that we can achieve a flexible engineering of superradiant, Fano-type, and subradiant resonances. Similar symmetric periodic array-like nanobowls and nanocavities with an interesting directional SERS effect have been reported.[47] In fact, the directional optical properties and the flexibly engineered line shapes may provide a great opportunity of using such kinds of substrates as plasmonic photonic crystals or directional couplers.[48] To further explore the optical properties of the fabricated structures for dedicated applications, we measured the structural orientation angle (φ) and polarization (ψ) dependent properties by our home-built spectroscopic system. Since the reflectance spectra of array $4^{\#}$ show a sharp SPR peak with a clear dependence on the incident angle, it would be interesting to investigate the effect of the substrate structural orientation on the optical properties of the substrate. The structural orientation angle φ is defined as the angle between the in-plane vector of the incident light k_0 and structural vector k_s that is pointing from the center of one cell to another (see Figure 3g). The reflectance spectra at four characteristic φ angles with an incidence angle set as 7.9° are shown in Figure 5a–d. Almost identical spectra were obtained at 0° and 60° (Figure 5a and c). Similar results can be observed for 30° and 90° cases (Figure 5b and d). The reflectance spectra over the whole φ range with steps of 10° are shown in Figure 5e (see the diagram in Figure S8 for s- and p-polarized light). This phenomenon can be understood by the 6-fold symmetry of the hexagonal array of the substrate. Furthermore, the uniformity of the structure over a large area also contributes to such a transformation trend.

We then investigated the optical properties of array $4^{\#}$ using a polarized light by tuning the polarization angle (ψ) (defined in Figure 3g). It is clear in Figure 3g that the polarization angle of $\psi = 90°$ corresponds to the condition of p polarization, while the angle of $\psi = 0°$ corresponds to s polarization. The spectra obtained at two structural orientation angles with p and s polarizations are shown in Figure 6b and e. For comparison, the

DOI: 10.1021/acsphotonics.5b00650
ACS Photonics 2015, 2, 1725–1731

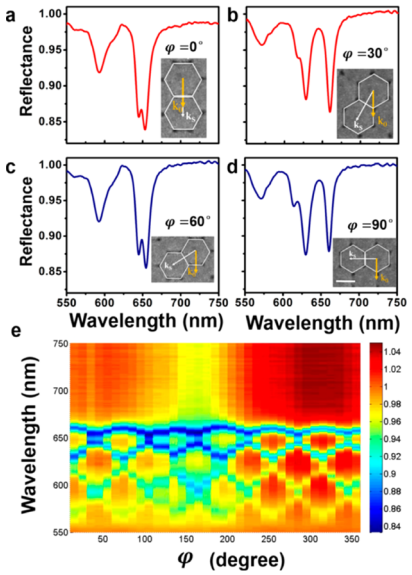

Figure 5. Dependence of the optical properties on the structural orientation angle φ defined in Figure 3g illuminated with an unpolarized white light for array 4#. The reflectance spectra were obtained at (a) 0°, (b) 30°, (c) 60°, and (d) 90°. (e) Plot of the reflectance spectra with the structural orientation angle φ over the whole angle range of 0° to 360°. The incidence angle is set as 7.9°.

spectra obtained with unpolarized light are given in Figure 6a and d. It is interesting to find that the spectrum in Figure 6a is the sum of the two spectra obtained at the two orientations in Figure 6b, and that in Figure 6c is the sum of the two spectra in Figure 6d. When the polarization angle was gradually changed from 0° to 360°, the reflectance spectra show a periodic change with the polarization angle with a period of 180°, as can be seen in Figure 6c and f. The positions of the dips are fixed, while some modes will completely disappear at a specific polarization. All the reflectance spectra shown in Figure 6 were measured with an incident angle of 7.9°; similar results can be found for other incident angles (see Figure S9). Such a sensitive polarization-dependent property suggests that the plasmonic nanoarrays can be used for the detection of the polarization of an unknown light source as well as other polarization-related applications.[49,50] We have demonstrated the interesting properties of array 4# regarding the incident angle, structural orientation angle, and polarization angle. More studies related to the application of the unique optical properties are under way and will be the topic of future publications. It is worth mentioning that the diameter of the excitation beam used in all the measurements is as large as 5 mm. In considering that the defects are usually unavoidable in an experimental work, it is quite impressive that we can still obtain such a perfect optical response in the polarization-dependent measurement, indicating the advantage of our method in fabrication of highly ordered structures.

CONCLUSION

In conclusion, we have fabricated a series of plasmonic nanostructures with tunable optical properties by the HL method. The SPR line shape has been successfully engineered by tuning the morphology of the plasmonic arrays via the convenient control of the exposure time. We have been able to obtain SPR features from sharp, to Fano-type resonances, and to broad line shapes. We further demonstrated that the optical properties of the plasmonic arrays critically depend on the incidence angle θ, the structural orientation angle φ, and the polarization angle ψ, which provides great opportunity for further applications. We anticipate that the broad line shape will be beneficial to achieve a high activity for surface-enhanced spectroscopy, and a substrate with a narrow line shape will be advantageous for SPR biosensing. Both topics are now ongoing in our lab. With the ability to fabricate periodic and uniform substrates in a large area with a high throughput, and the flexibility to tune the morphology, period, and material of the plasmonic structures, HL may be a promising method to fabricate plasmonic structures with anticipated applications.

MATERIAL AND METHODS

Fabrication of the Hexagonal Nanopillar Array. Silicon single-crystal wafers were sonicated in acetone and ethanol for 10 min successively. Then, they were soaked in piranha solution (H_2SO_4/H_2O_2 = 3:1, volume ratio) for 30 min and rinsed with deionized water. After drying, the clean Si wafers were coated with a 400 nm thick layer of SU-8 2000.5 photoresist (MicroChem). The prepared substrates were then exposed to a 266 nm laser using the HL method, followed by development with propylene glycol methyl ether acetate. Afterward, a 2 nm Cr adhesion layer was deposited prior to a 100 nm Au layer using electron-beam evaporation (Temescal, FC-2000).

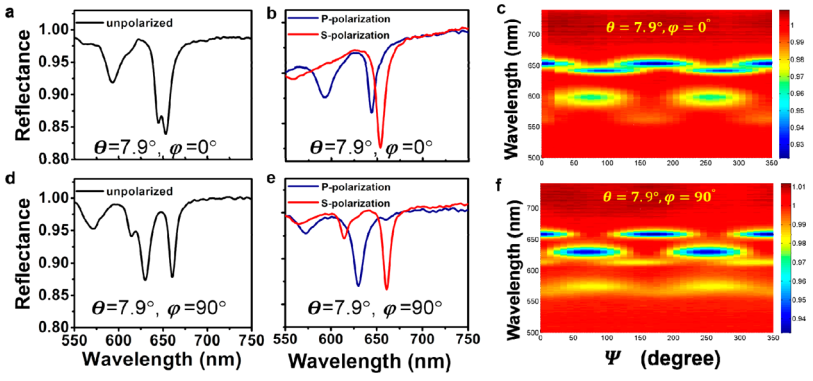

Figure 6. Polarization angle (ψ) dependent reflectance spectra obtained on array 4# for two structural orientations of 0° for (a), (b), and (c) and 90° for (d), (e), and (f). (a) and (d) were obtained with unpolarized light, and (b) and (e) were obtained with s- and p-polarized light. (c) and (f) are plots of the reflectance spectra with the change of the polarization angle ψ. All the spectra were acquired at an incidence angle of 7.9°. ψ is defined in Figure 3g.

DOI: 10.1021/acsphotonics.5b00650
ACS Photonics 2015, 2, 1725−1731

Reflectance Spectroscopy. The normal, oblique incident, and the angle-resolved reflectance measurements were carried out on a home-built system (see Figure S4 in the Supporting Information), including a PI spectrometer (Princeton Instruments, IsoPlane SCT320), a light source (Avantes, AvaLight-DH-S-BAL), and a mechanical rotating platform (see Figures S5 and S6 in the Supporting Information).

■ ASSOCIATED CONTENT

Supporting Information

The Supporting Information is available free of charge on the ACS Publications website at DOI: 10.1021/acsphotonics.5b00650.

The principle of HL, schematic and photograph of the holographic optical element (HOE), the home-built angle-resolved reflectance spectroscopic system, fitting result of the narrow SPR mode on array 4# (Figure 4d) with theoretical SPP mode, dependence of the reflectance spectra on the structural orientation angle and the polarization of the incident light (PDF)

■ AUTHOR INFORMATION

Corresponding Authors

*E-mail: wanglei33@xmu.edu.cn.
*E-mail: bren@xmu.edu.cn.

Notes

The authors declare no competing financial interest.

■ ACKNOWLEDGMENTS

We acknowledge the funding and support from MOST (2013CB933703 and 2011YQ03012400), NSFC (21373173, 21321062, 21227004, and J1310024), and the Fundamental Research Funds for the Central Universities (2010121019).

■ REFERENCES

(1) Schuller, J. A.; Barnard, E. S.; Cai, W.; Jun, Y. C.; White, J. S.; Brongersma, M. L. Plasmonics for extreme light concentration and manipulation. *Nat. Mater.* **2010**, *9*, 193−204.

(2) Luk'yanchuk, B.; Zheludev, N. I.; Maier, S. A.; Halas, N. J.; Nordlander, P.; Giessen, H.; Chong, C. T. The Fano resonance in plasmonic nanostructures and metamaterials. *Nat. Mater.* **2010**, *9*, 707−715.

(3) Sonnefraud, Y.; Verellen, N.; Sobhani, H.; Vandenbosch, G. A. E.; Moshchalkov, V. V.; Van Dorpe, P.; Nordlander, P.; Maier, S. A. Experimental Realization of Subradiant, Superradiant, and Fano Resonances in Ring/Disk Plasmonic Nanocavities. *ACS Nano* **2010**, *4*, 1664−1670.

(4) Kelly, K. L.; Coronado, E.; Zhao, L. L.; Schatz, G. C. The optical properties of metal nanoparticles: The influence of size, shape, and dielectric environment. *J. Phys. Chem. B* **2003**, *107*, 668−677.

(5) Kravets, V. G.; Schedin, F.; Grigorenko, A. N. Extremely narrow plasmon resonances based on diffraction coupling of localized plasmons in arrays of metallic nanoparticles. *Phys. Rev. Lett.* **2008**, *101*, 101.

(6) Le, F.; Brandl, D. W.; Urzhumov, Y. A.; Wang, H.; Kundu, J.; Halas, N. J.; Aizpurua, J.; Nordlander, P. Metallic nanoparticle arrays: A common substrate for both surface-enhanced Raman scattering and surface-enhanced infrared absorption. *ACS Nano* **2008**, *2*, 707−718.

(7) Hao, F.; Nordlander, P.; Sonnefraud, Y.; Van Dorpe, P.; Maier, S. A. Tunability of Subradiant Dipolar and Fano-Type Plasmon Resonances in Metallic Ring/Disk Cavities: Implications for Nanoscale Optical Sensing. *ACS Nano* **2009**, *3*, 643−652.

(8) Liu, N.; Langguth, L.; Weiss, T.; Kastel, J.; Fleischhauer, M.; Pfau, T.; Giessen, H. Plasmonic analogue of electromagnetically induced transparency at the Drude damping limit. *Nat. Mater.* **2009**, *8*, 758−762.

(9) Lassiter, J. B.; Sobhani, H.; Fan, J. A.; Kundu, J.; Capasso, F.; Nordlander, P.; Halas, N. J. Fano Resonances in Plasmonic Nanoclusters: Geometrical and Chemical Tunability. *Nano Lett.* **2010**, *10*, 3184−3189.

(10) Gallinet, B.; Siegfried, T.; Sigg, H.; Nordlander, P.; Martin, O. J. F. Plasmonic Radiance: Probing Structure at the Angstrom Scale with Visible Light. *Nano Lett.* **2013**, *13*, 497−503.

(11) Gottheim, S.; Zhang, H.; Govorov, A. O.; Halas, N. J. Fractal Nanoparticle Plasmonics: The Cayley Tree. *ACS Nano* **2015**, *9*, 3284−3292.

(12) Gallinet, B.; Martin, O. J. F. Influence of Electromagnetic Interactions on the Line Shape of Plasmonic Fano Resonances. *ACS Nano* **2011**, *5*, 8999−9008.

(13) Liu, N.; Weiss, T.; Mesch, M.; Langguth, L.; Eigenthaler, U.; Hirscher, M.; Soennichsen, C.; Giessen, H. Planar Metamaterial Analogue of Electromagnetically Induced Transparency for Plasmonic Sensing. *Nano Lett.* **2010**, *10*, 1103−1107.

(14) Min, B.; Ostby, E.; Sorger, V.; Ulin-Avila, E.; Yang, L.; Zhang, X.; Vahala, K. High-Q surface-plasmon-polariton whispering-gallery microcavity. *Nature* **2009**, *457*, 455−458.

(15) Noginov, M. A.; Zhu, G.; Belgrave, A. M.; Bakker, R.; Shalaev, V. M.; Narimanov, E. E.; Stout, S.; Herz, E.; Suteewong, T.; Wiesner, U. Demonstration of a spaser-based nanolaser. *Nature* **2009**, *460*, 1110−1112.

(16) Suh, J. Y.; Kim, C. H.; Zhou, W.; Huntington, M. D.; Co, D. T.; Wasielewski, M. R.; Odom, T. W. Plasmonic Bowtie Nanolaser Arrays. *Nano Lett.* **2012**, *12*, 5769−5774.

(17) Zhou, W.; Odom, T. W. Tunable subradiant lattice plasmons by out-of-plane dipolar interactions. *Nat. Nanotechnol.* **2011**, *6*, 423−427.

(18) Yanik, A. A.; Cetin, A. E.; Huang, M.; Artar, A.; Mousavi, S. H.; Khanikaev, A.; Connor, J. H.; Shvets, G.; Altug, H. Seeing protein monolayers with naked eye through plasmonic Fano resonances. *Proc. Natl. Acad. Sci. U. S. A.* **2011**, *108*, 11784−11789.

(19) Shen, Y.; Zhou, J. H.; Liu, T. R.; Tao, Y. T.; Jiang, R. B.; Liu, M. X.; Xiao, G. H.; Zhu, J. H.; Zhou, Z. K.; Wang, X. H.; Jin, C. J.; Wang, J. F. Plasmonic gold mushroom arrays with refractive index sensing figures of merit approaching the theoretical limit. *Nat. Commun.* **2013**, *4*, 2381.

(20) Sherry, L. J.; Chang, S. H.; Schatz, G. C.; Van Duyne, R. P.; Wiley, B. J.; Xia, Y. N. Localized surface plasmon resonance spectroscopy of single silver nanocubes. *Nano Lett.* **2005**, *5*, 2034−2038.

(21) Atwater, H. A.; Polman, A. Plasmonics for improved photovoltaic devices. *Nat. Mater.* **2010**, *9*, 205−213.

(22) Pala, R. A.; White, J.; Barnard, E.; Liu, J.; Brongersma, M. L. Design of Plasmonic Thin-Film Solar Cells with Broadband Absorption Enhancements. *Adv. Mater.* **2009**, *21*, 3504−3509.

(23) Ferry, V. E.; Verschuuren, M. A.; van Lare, M. C.; Schropp, R. E. I.; Atwater, H. A.; Polman, A. Optimized Spatial Correlations for Broadband Light Trapping Nanopatterns in High Efficiency Ultrathin Film a-Si:H Solar Cells. *Nano Lett.* **2011**, *11*, 4239−4245.

(24) Chen, X.; Jia, B. H.; Saha, J. K.; Cai, B. Y.; Stokes, N.; Qiao, Q.; Wang, Y. Q.; Shi, Z. R.; Gu, M. Broadband Enhancement in Thin-Film Amorphous Silicon Solar Cells Enabled by Nucleated Silver Nanoparticles. *Nano Lett.* **2012**, *12*, 2187−2192.

(25) Maier, S. A. The benefits of darkness. *Nat. Mater.* **2009**, *8*, 699−700.

(26) Hentschel, M.; Saliba, M.; Vogelgesang, R.; Giessen, H.; Alivisatos, A. P.; Liu, N. Transition from Isolated to Collective Modes in Plasmonic Oligomers. *Nano Lett.* **2010**, *10*, 2721−2726.

(27) Verellen, N.; Sonnefraud, Y.; Sobhani, H.; Hao, F.; Moshchalkov, V. V.; Van Dorpe, P.; Nordlander, P.; Maier, S. A. Fano Resonances in Individual Coherent Plasmonic Nanocavities. *Nano Lett.* **2009**, *9*, 1663−1667.

(28) Li, Z. P.; Zhang, S. P.; Tong, L. M.; Wang, P. J.; Dong, B.; Xu, H. X. Ultrasensitive Size-Selection of Plasmonic Nanoparticles by Fano Interference Optical Force. *ACS Nano* **2014**, *8*, 701−708.

DOI: 10.1021/acsphotonics.5b00650
ACS Photonics 2015, 2, 1725−1731

(29) Rahmani, M.; Lei, D. Y.; Giannini, V.; Lukiyanchuk, B.; Ranjbar, M.; Liew, T. Y. F.; Hong, M. H.; Maier, S. A. Subgroup Decomposition of Plasmonic Resonances in Hybrid Oligomers: Modeling the Resonance Lineshape. *Nano Lett.* **2012**, *12*, 2101−2106.
(30) Zhan, Y. H.; Lei, D. Y.; Li, X. F.; Maier, S. A. Plasmonic Fano resonances in nanohole quadrumers for ultra-sensitive refractive index sensing. *Nanoscale* **2014**, *6*, 4705−4715.
(31) Lassiter, J. B.; Sobhani, H.; Knight, M. W.; Mielczarek, W. S.; Nordlander, P.; Halas, N. J. Designing and Deconstructing the Fano Lineshape in Plasmonic Nanoclusters. *Nano Lett.* **2012**, *12*, 1058−1062.
(32) Schmidt, M. A.; Lei, D. Y.; Wondraczek, L.; Nazabal, V.; Maier, S. A. Hybrid nanoparticle-microcavity-based plasmonic nanosensors with improved detection resolution and extended remote-sensing ability. *Nat. Commun.* **2012**, *3*, 1108.
(33) Hentschel, M.; Dregely, D.; Vogelgesang, R.; Giessen, H.; Liu, N. Plasmonic Oligomers: The Role of Individual Particles in Collective Behavior. *ACS Nano* **2011**, *5*, 2042−2050.
(34) Wu, C.; Khanikaev, A. B.; Adato, R.; Arju, N.; Yanik, A. A.; Altug, H.; Shvets, G. Fano-resonant asymmetric metamaterials for ultrasensitive spectroscopy and identification of molecular monolayers. *Nat. Mater.* **2012**, *11*, 69−75.
(35) Li, Z. Y.; Butun, S.; Aydin, K. Ultranarrow Band Absorbers Based on Surface Lattice Resonances in Nanostructured Metal Surfaces. *ACS Nano* **2014**, *8*, 8242−8248.
(36) Lei, D. Y.; Li, J.; Fernandez-Dominguez, A. I.; Ong, H. C.; Maier, S. A. Geometry Dependence of Surface Plasmon Polariton Lifetimes in Nanohole Arrays. *ACS Nano* **2010**, *4*, 432−438.
(37) Ho, Y. L.; Portela, A.; Lee, Y.; Maeda, E.; Tabata, H.; Delaunay, J. J. Hollow Plasmonic U-Cavities with High-Aspect-Ratio Nanofins Sustaining Strong Optical Vortices for Light Trapping and Sensing. *Adv. Opt. Mater.* **2014**, *2*, 522−528.
(38) Do, Y. S.; Park, J. H.; Hwang, B. Y.; Lee, S. M.; Ju, B. K.; Choi, K. C. Plasmonic Color Filter and its Fabrication for Large-Area Applications. *Adv. Opt. Mater.* **2013**, *1*, 133−138.
(39) Mao, W.; Wathuthanthri, I.; Choi, C.-H. Tunable two-mirror interference lithography system for wafer-scale nanopatterning. *Opt. Lett.* **2011**, *36*, 3176−3178.
(40) Campbell, M.; Sharp, D. N.; Harrison, M. T.; Denning, R. G.; Turberfield, A. J. Fabrication of photonic crystals for the visible spectrum by holographic lithography. *Nature* **2000**, *404*, 53−56.
(41) Berger, V.; GauthierLafaye, O.; Costard, E. Photonic band gaps and holography. *J. Appl. Phys.* **1997**, *82*, 60−64.
(42) Miklyaev, Y. V.; Meisel, D. C.; Blanco, A.; von Freymann, G.; Busch, K.; Koch, W.; Enkrich, C.; Deubel, M.; Wegener, M. Three-dimensional face-centered-cubic photonic crystal templates by laser holography: fabrication, optical characterization, and band-structure calculations. *Appl. Phys. Lett.* **2003**, *82*, 1284−1286.
(43) Lee, S. K.; Park, H. S.; Yi, G. R.; Moon, J. H.; Yang, S. M. Holographic Fabrication of Microstructures with Internal Nano-patterns Using Microprism Arrays. *Angew. Chem., Int. Ed.* **2009**, *48*, 7000−7005.
(44) Jeon, H. C.; Heo, C. J.; Lee, S. Y.; Park, S. G.; Yang, S. M. Optically tunable arrayed structures for highly sensitive plasmonic detection via simplified holographic lithography. *J. Mater. Chem.* **2012**, *22*, 4603−4606.
(45) Bagheri, S.; Giessen, H.; Neubrech, F. Large-Area Antenna-Assisted SEIRA Substrates by Laser Interference Lithography. *Adv. Opt. Mater.* **2014**, *2*, 1050−1056.
(46) Zhang, X.; Theuring, M.; Song, Q.; Mao, W. D.; Begliarbekov, M.; Strauf, S. Holographic Control of Motive Shape in Plasmonic Nanogap Arrays. *Nano Lett.* **2011**, *11*, 2715−2719.
(47) Baumberg, J. J.; Kelf, T. A.; Sugawara, Y.; Cintra, S.; Abdelsalam, M. E.; Bartlett, P. N.; Russell, A. E. Angle-resolved surface-enhanced Raman scattering on metallic nanostructured plasmonic crystals. *Nano Lett.* **2005**, *5*, 2262−2267.
(48) Liu, T. R.; Shen, Y.; Shin, W.; Zhu, Q. Z.; Fan, S. H.; Jin, C. J. Dislocated Double-Layer Metal Gratings: An Efficient Unidirectional Coupler. *Nano Lett.* **2014**, *14*, 3848−3854.
(49) Li, Z. P.; Shegai, T.; Haran, G.; Xu, H. X. Multiple-Particle Nanoantennas for Enormous Enhancement and Polarization Control of Light Emission. *ACS Nano* **2009**, *3*, 637−642.
(50) Lovera, P.; Jones, D.; Corbett, B.; O'Riordan, A. Polarization tunable transmission through plasmonic arrays of elliptical nanopores. *Opt. Express* **2012**, *20*, 25325−25332.

DOI: 10.1021/acsphotonics.5b00650
ACS Photonics 2015, 2, 1725−1731